Heading Estimation for Multimode Pedestrian Dead Reckoning

Lingxiao Zheng, Xingqun Zhan, *Senior Member, IEEE*, Xin Zhang, Shizhuang Wang, *Member, IEEE*, and Wenhan Yuan

***Abstract*—The flexible carrying mode of smartphone brings challenge for Pedestrian Dead Reckoning (PDR) especially for heading estimation with build-in sensors. This paper focuses on POCKET mode and SWING mode and analyzes the correlation between smartphone's rotational motion and pedestrian's walking cycle states and walking direction. Based on the analysis, we propose to use the rotation vector sensor data of smartphone within one walking step to estimate the pedestrian's heading. For POCKET mode, heading is estimated by an improved rotational approach (IRA). A jitter detection algorithm is proposed to extract leg flexion interval. Stable walking direction without 180° ambiguity is obtained from the averaged rotation axis. For SWING mode, a single-point (SP) method is proposed. Heading is estimated from the direction of smartphone's y-axis when it is closest to the horizontal plane. The algorithms are validated with data collected by HUAWEI mate 10 smartphone. The RMS errors are less than 4.37° and 3.38° for POCKET and SWING mode respectively. Superior to previous heading estimation algorithms, our method can converge within one single walking step for both carrying modes without 180° ambiguity.**

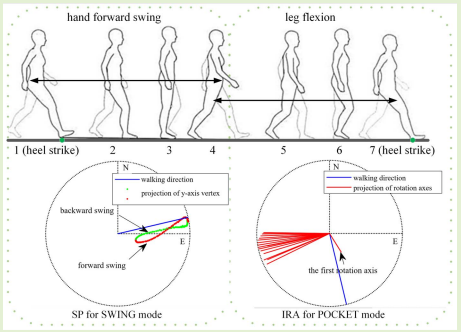

***Index Terms*—Pedestrian dead reckoning, heading estimation, multi-mode, smartphone.**

I. Introduction

LOCATION based services (LBS) facilitate people's daily lives in many mobile applications. Real-time on-board continuous pedestrian tracking is seen as key technology for LBS [1]. For open sky outdoor environment, Global Navigation Satellite System (GNSS) provides good results. But the performance of GNSS deteriorates significantly in indoor environment due to signal attenuation [2], [3].

Pedestrian Dead Reckoning methods using motion sensors are attractive solutions since they do not depend on any infrastructure compared to other indoor positioning methods based on optical motion tracking [4] or wireless signal positioning [5]. Micro-Electro-Mechanical System (MEMS) Inertial Measurement Units (IMUs) are particularly suitable for pedestrian tracking. They are small, light and low cost that makes them wearable or portable. Alongside the dedicated IMU, the widely used smartphones also integrate different motion and environment sensors with powerful processing capability. Naturally, smartphone becomes an ideal platform for indoor pedestrian tracking.

A lot of wearable PDR systems are verified in literatures including foot-mounted and waist-mounted system with different levels of MEMS IMUs [6]–[8]. The basic idea of the inertial-based PDR for pedestrian tracking using IMU is an application of the well-known Strapdown Inertial Navigation (SIN) algorithm. In order to compensate the accumulated errors caused by sensor drift and noise, stance phase detection and Zero-velocity Update (ZUPT) are employed for foot-mounted inertial-based PDR [9], [10].

But when it comes to smartphone, hand-held is more common and thus periodic zero-velocity constraints are no longer applicable. Step-based PDR is widely employed for hand-held tracking problem. Step detection, step length estimation, heading estimation and position update are four core modules for step-based PDR. Peak detection, zero crossing, template matching and spectral analysis are typical techniques for the step detection [11]. Patterns in the sensor signal are used to estimate the step length instead of acceleration double integration [12]. For heading estimation, the yaw angle of the smartphone is applied when it is held and direct in front of the user's body [13], [14]. Many researchers focus on eliminating the cumulative error caused by incorrect step length and heading estimation using external information, benefiting from the various sensors embedded in smartphones [15]–[18].

Manuscript received January 16, 2020; revised March 18, 2020; accepted March 29, 2020. Date of publication April 2, 2020; date of current version July 6, 2020. This work was supported in part by the National Natural Science Foundation of China under Grant 61403253. The associate editor coordinating the review of this article and approving it for publication was Dr. Ashish Pandharipande. *(Corresponding author: Xingqun Zhan.)*

The authors are with the School of Aeronautics and Astronautics, Shanghai Jiao Tong University, Shanghai 200240, China (e-mail: lx_zheng@sjtu.edu.cn; xqzhan@sjtu.edu.cn; xin.zhang@sjtu.edu.cn; sz.wang@sjtu.edu.cn; luokerenxxz@sjtu.edu.cn).

Digital Object Identifier 10.1109/JSEN.2020.2985025

However, the challenge for heading estimation of the step-based PDR using smartphone is the fact that the carrying mode may vary in practical applications. Among three typical carrying modes [19], [20], HOLDING is the mode that user holds the phone in front of body, which is the situation of traditional hand-held PDR. POCKET is that the phone is placed in the front trouser pocket while walking. SWING is that phone is held in hand and swung beside body. In POCKET and SWING, it is not appropriate to use the yaw angle of smartphone to represent the heading of walking. Several methods are proposed in related work to address this limitation.

In [20], an averaging technique with adaptive offset compensation (AOC) scheme is developed to process the yaw angle to get an accurate heading for multi-mode PDR system. This method assumes that the initial mode is HOLDING and the walking direction remains the same before and after mode transition during the offset training stage.

In [21], several unconstrained heading estimation methods for POCKET mode PDR are evaluated. The rotational approach (RA) exploits the observation that the rotation of the device in trouser pocket is coupled with the thigh's rotation, and the rotation axis is approximately orthogonal to pedestrian's heading. The principal component analysis (PCA) based approaches [21], [22] utilize the correlation between user's motion axis and the first eigenvector of the horizontal east and north accelerations. There is a 180° ambiguity in PCA-based heading because the first eigenvector may point to the forward or backward of the pedestrian.

In [23], a PCA-based method with global accelerations (PCA-GA) is implemented on the data of smartphone fixed three-axis accelerometer. The third eigenvector is used to infer the orthogonal direction of walking in smartphone coordinate fame. Gravity and magnetic vector are used to transform this orthogonal direction into navigation frame.

Both the AOC scheme and the PCA-based methods require several walking steps to get a stable heading estimation. Thus, the heading output of these algorithms are not reliable in quite many steps when the walking direction changes at one certain walking step. The heading estimation accuracy of RA is relatively poor because the rotation axis calculation does not consider the influence of human walking cycle states such as heel strike, leg flexion and leg extension. The PCA-GA method only uses accelerometer and magnetometer to calculate the smartphone's attitude reference for transforming the walking direction into navigation frame. The heading estimation error is quite large due to the influence of linear acceleration and magnetic field disturbance. Actually, many smartphones now include gyroscope. Software-based motion sensors of smartphone such as gravity sensor and rotation vector sensor can provide better attitude reference by fusing data from accelerometer, magnetometer and gyroscope [24].

Considering the above limitations of the existing multi-mode heading estimation methods in practical applications, designing a new pedestrian heading estimation method based on rotation vector sensor that can converge in one single walking step is the objective of our work.

The remainder of this paper is organized as follows. The heading estimation problem for multi-mode PDR is shown in Section II. The proposed heading estimation methods for POCKET mode and SWING mode are presented in Section III. Our approach and three PCA-based algorithms using data within one walking step are implemented to process the collected data. The results are shown in Section IV. Theoretical comparison with the original rotational approach (RA) is also provided in this section. Finally, conclusion remarks and future work are presented in Section V.

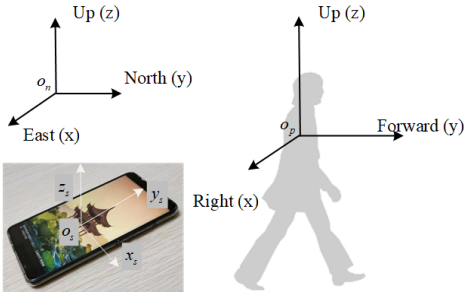

Fig. 1. Coordinate frame of navigation reference, pedestrian and smartphone.

II. Heading Estimation Problem

The navigation coordinate frame, pedestrian coordinate frame and smartphone coordinate frame used in this paper are defined as follows in Fig. 1.

Pedestrian only rotates about the Up axis. The orientation can be described by the heading angle $\chi \in (-\pi, +\pi]$ or direction cosine vector $\boldsymbol{\chi} = [-\sin\chi \ \cos\chi]$. χ is the angle formed from the North to pedestrian's forward-axis and the sign is defined by right hand rule. In this paper, it is assumed that the pedestrian's forward axis points to the walking direction. Walking sideways or walking in a circle are not considered in our current work.

The orientation of a smartphone can be described by direction cosine matrix, Euler angle, rotation vector and quaternion.

Direction cosine matrix $\boldsymbol{C}_s^n$ is an orthogonal matrix expressed by

$$\boldsymbol{C}_s^n = \begin{bmatrix} \boldsymbol{u}_1 & \boldsymbol{u}_2 & \boldsymbol{u}_3 \end{bmatrix} \tag{1}$$

whose columns indicate the position of smartphone axes in navigation frame. Each element of $\boldsymbol{C}_s^n$ is the cosine of the angle formed by one of the smartphone's axes with one of the navigation frame's axes [25].

Euler angles describe the orientation using three sequential rotations around pre-defined axes from navigation frame to get to the position of smartphone frame. The yaw, pitch and roll denoted as ψ, θ and φ is one set of the common used Euler angles. The transformation between this set of Euler angles and direction cosine matrix is given by

$$\boldsymbol{C}_s^n = \begin{bmatrix} \mathrm{c}\varphi\mathrm{c}\psi - \mathrm{s}\varphi\mathrm{s}\psi\mathrm{s}\theta & -\mathrm{s}\psi\mathrm{c}\theta & \mathrm{c}\psi\mathrm{s}\varphi + \mathrm{s}\psi\mathrm{s}\theta\mathrm{c}\varphi \\ \mathrm{s}\psi\mathrm{c}\varphi + \mathrm{c}\psi\mathrm{s}\theta\mathrm{s}\varphi & \mathrm{c}\psi\mathrm{c}\theta & \mathrm{s}\psi\mathrm{s}\varphi - \mathrm{c}\psi\mathrm{s}\theta\mathrm{c}\varphi \\ -\mathrm{c}\theta\mathrm{s}\varphi & \mathrm{s}\theta & \mathrm{c}\theta\mathrm{c}\varphi \end{bmatrix} \tag{2}$$

where c stands for cos and s stands for sin. It is easily verified from (1) and (2) that yaw angle ψ is the angle formed between the North and the smartphone's y-axis horizontal projection when $\cos(\theta)$ is not equal to zero.

Rotation vector $\boldsymbol{\phi}$ encodes the orientation as a single rotation with a unit rotation axis $\boldsymbol{u}$ and rotation angle ϕ, where $\boldsymbol{\phi} = \phi\boldsymbol{u}$. The transformation between rotation vector and direction cosine matrix is given by (3). $(\cdot)\times$ donates skew symmetric matrix form of the preceding vector. When ϕ equals to 0, the corresponding $\boldsymbol{C}_s^n$ is an identity matrix [26].

$$\boldsymbol{C}_s^n = \boldsymbol{I} + \frac{\sin\phi}{\phi}(\boldsymbol{\phi}\times) + \frac{1-\cos\phi}{\phi^2}(\boldsymbol{\phi}\times)^2 \tag{3}$$

A more commonly used four parameters rotation vector is the quaternion. The transformation between rotation vector $\boldsymbol{\phi}$ and quaternion $\boldsymbol{q}_s^n$ is shown in (4). When ϕ equals to 0, the corresponding $\boldsymbol{q}_s^n$ is an identity vector $[1\ 0\ 0\ 0]^{\mathrm{T}}$.

$$\boldsymbol{q}_s^n = \begin{bmatrix} \cos\dfrac{\phi}{2} \\ \dfrac{\boldsymbol{\phi}}{\phi}\sin\dfrac{\phi}{2} \end{bmatrix} \tag{4}$$

Fig.2 shows the orientation of smartphone's y-axis under three typical carrying modes when walking along the same direction. Line with blue color represents the unit vector along smartphone's y-axis. The left column shows the trajectory of this vector in navigation frame. The right column shows the trajectory's projection on horizontal plane. As seen from the right column, in HOLDING mode, yaw angle of smartphone is almost constant during one step when walking straight. But in POCKET and SWING modes, there are obvious oscillations.

The difficulty in heading estimation of multi-mode PDR is that the deviation between pedestrian's heading and smartphone's yaw angle is variable and unknown.

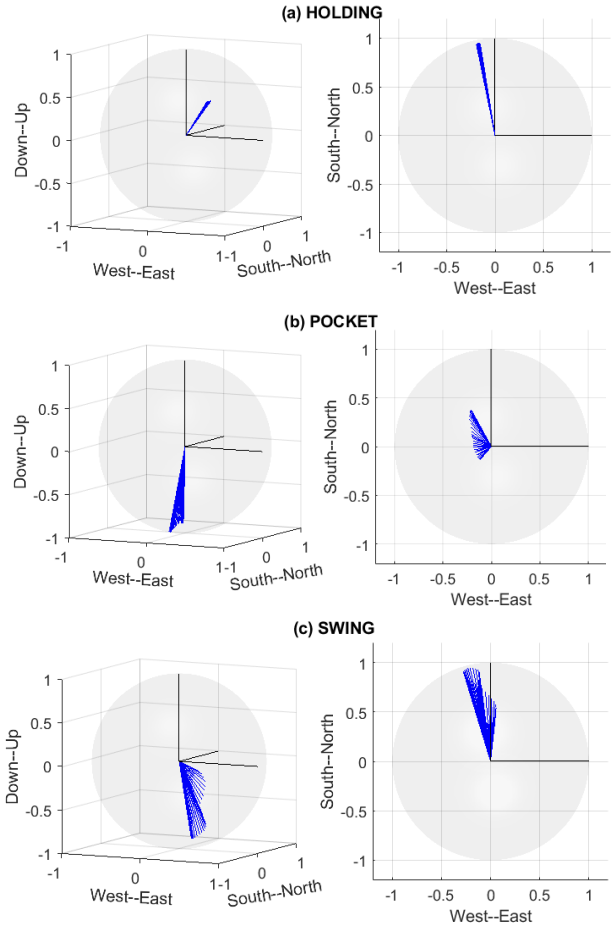

Fig. 2. Orientation of smartphone's y-axis in different modes.

III. Proposed Heading Estimation Method

A. Rotation Vector Sensor

Rotation vector sensor is a software-based sensor in smartphone. It provides the estimation of a smartphone's orientation by fusing the raw sensor data from accelerometer, magnetometer and gyroscope.

The orientation of smartphone can be reconstructed from accelerometer and magnetometer. But the linear acceleration of smartphone and magnetic disturbance will lead to poor error characterization.

On the other hand, the orientation of smartphone can be computed by numerically integrating the gyroscope measurement provided that the initial condition is known. But the initial condition error and gyroscope measurement bias and noise make the error accumulated.

Fusion algorithm based on gradient descent algorithm [27] or complementary filter [28], [29] can provide computationally efficient orientation estimation for portable application. Data from gyroscope is used to filter out the high frequency error in the reconstructed orientation from accelerometer and magnetometer. Data from accelerometer and magnetometer is used to compensate the error caused by bias of gyroscope measurement and initial condition error.

The output of the rotation vector sensor in smartphone is usually in quaternion representation. Therefore, the input of the algorithms proposed in our paper is also in quaternion representation.

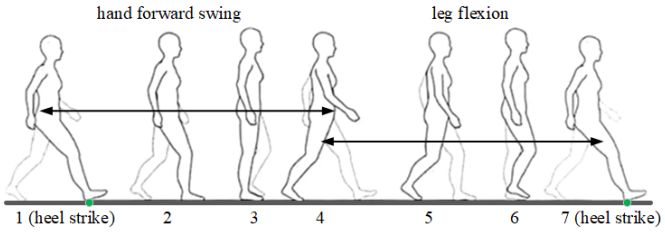

Fig. 3. Human walking cycle of one step.

B. Walking Cycle State Detection

This part analyzes the correlation between the pedestrian's walking cycle and the smartphone's inclination rotational motion under POCKET and SWING. Based on the analysis, the walking cycle states, including heel strike, leg flexion interval and hand forward swing interval, are detected.

All the information required for heading estimation proposed in this paper is just within time of one walking step. One walking step refers to the process that one of the heels strikes the ground two consecutive times as shown in Fig. 3. Process $1 \sim 4$ correspond to the leg extension and the hand forward swing. Process $4 \sim 7$ correspond to the leg flexion and the hand backward swing.

Fig.4 shows the data collection system for motion analysis. A 3DM-GX3-25 MEMS IMU is attached to the ankle with an

Fig. 4. Data collection system for motion analysis.

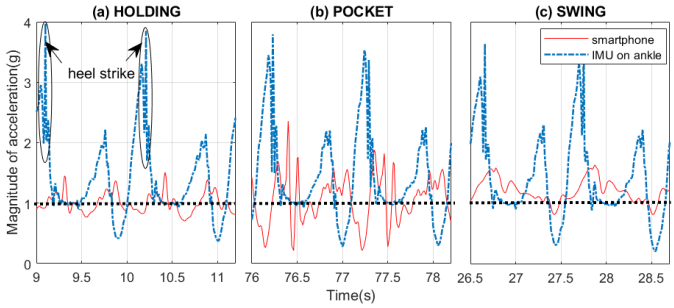

Fig. 5. Magnitude of acceleration in different modes.

elastic band and its data is logged to the data logger placed in backpack. A Huawei Mate 10 smartphone is carried in POCKET mode and SWING mode respectively and the data is collected in smartphone's storage card. The clocks of IMU data logger and the smartphone are synchronized to UTC time.

Each time the heel strikes the ground, the IMU mounted on ankle captures a distinct acceleration peak as shown in Fig.5. But for smartphone, to detect the heel strike state, low pass filter and threshold strategies are required to process the peaks in the magnitude of acceleration [19], [20]. Besides, for different carrying modes and different people, it's difficult to find a uniform threshold.

Actually, in POCKET and SWING mode, there is a correlation between pedestrian's walk cycle and the smartphone's rotational motion, especially the inclination rotational motion. This makes it possible to detect walking cycle states without complex threshold design.

The vector in the third row of direction cosine matrix in (2) describes the inclination orientation of smartphone. It should be noted that the relationship between this vector and the normalized gravity vector in smartphone frame [30] is

$$\boldsymbol{v}_{g^s} = \frac{\boldsymbol{g}^s}{|\boldsymbol{g}|} = -\left[-\mathrm{c}\theta\mathrm{s}\varphi \quad \mathrm{s}\theta \quad \mathrm{c}\theta\mathrm{c}\varphi\right]^{\mathrm{T}} \tag{5}$$

Fig. 6 presents an example of the normalized 3-axis gravity vector components variation during walking in POCKET Mode. The dot dash line with blue color is the magnitude of acceleration captured from the ankle mounted IMU. It is used to mark the walk cycle.

In this example, the IMU and the smartphone are on the same leg. As shown in Fig.6, leg extension and the leg flexion

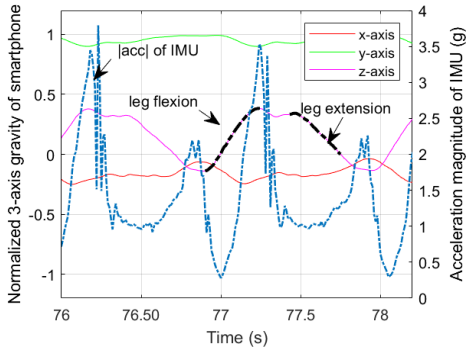

Fig. 6. Example of the normalized gravity vector in POCKET mode.

are the monotonous intervals between peak area and valley area of z-axis gravity. Fig.6 is the case when the smartphone is placed in the front trouser pocket with its screen facing the thigh. When only use peak and valley to detect step, the jitters in peak and valley area will lead to false step detection. Moreover, distinguishing the leg extension and leg flexion will be impossible because the peak area and valley area will upside down when the smartphone is placed with its back side facing the thigh.

Actually, the jitter is a useful feature. Jitter here is define as a signal interval in which the peaks and valleys have the same sign. The peak or valley area with longer jitter in z-axis gravity corresponds to the heel strike as shown in Fig. 6. Based on the above observation, this jitter can be used as a strong feature to segment per step and extract the leg flexion interval with no constraints on the way how the smartphone is placed in the pocket of front trouser.

Firstly, implement peak and valley detection algorithm on z-axis gravity by (6) with x_i denotes the sequence of z-axis gravity.

$$\begin{cases} x_i \text{ is peak value if } \mathrm{sign}\,(x_{i-1} - x_i) - \mathrm{sign}\,(x_i - x_{i+1}) < 0 \\ x_i \text{ is valley value if } \mathrm{sign}\,(x_{i-1} - x_i) - \mathrm{sign}\,(x_i - x_{i+1}) > 0 \end{cases} \tag{6}$$

Arrange the output peaks and valleys in the order they occur and still let x_i denotes this sequence. The jitter detection process is outlined as follows in (7).

$$\begin{cases} \text{jitter starts at indice } i & \text{if } \mathrm{sign}\,(x_i) = \mathrm{sign}\,(x_{i+1}) \\ \text{jitter ends at indice } j & \text{if } \mathrm{sign}\,(x_j) \neq \mathrm{sign}\,(x_{j+1}) \end{cases} \tag{7}$$

Then, the leg flexion interval is extracted from the monotonical change interval in the z-axis gravity before the heel strike.

When it comes to the SWING mode, the correlation between walking cycle and inclination rotational motion is direct. Fig. 7 shows an example of the normalized 3-axis gravity components variation in SWING Mode.

In this example, the IMU and the smartphone are in the same side of the foot and the hand. The y-axis of smartphone is point to the front of the hand. Thus, the y-axis gravity increases during backward swing and decrease during forward swing. Therefore, the peak and valley in y-axis gravity are exploited to segment per step and to extract the forward swing interval

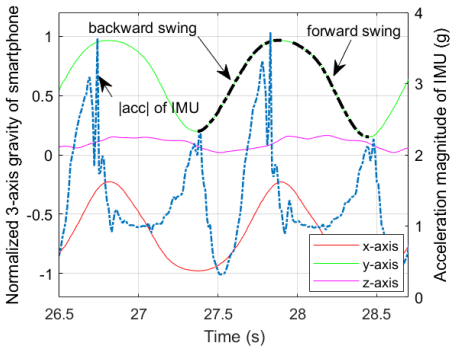

Fig. 7. Example of the normalized gravity vector in SWING mode.

under the constraint that y-axis is point to the front of the hand.

C. Improved Rotational Approach

To determine the heading of pedestrian using smartphone in pocket, the rotational approach in [21] proposes to estimate the heading using the correlation between smartphone's rotational motion and pedestrian's walking direction. But there are no details about the calculation process.

In our improved rational approach, after extracting leg flexion interval, use $[T_1, T_2, \ldots, T_m, \ldots, T_M]$ to denote the timestamps during leg flexion. Let quaternion $\boldsymbol{q}_{s_1}^n$ and $\boldsymbol{q}_{s_m}^n$ denote the orientation of the smartphone at the leg flexion start time T_1 and at subsequent time T_m. n and s represent the navigation frame and smartphone frame. Let quaternion $\boldsymbol{q}_{s_m}^{s_1}$ denote the orientation change from smartphone frame s_1 to s_m, which is given by

$$\boldsymbol{q}_{s_m}^{s_1} = \boldsymbol{q}_n^{s_1} \otimes \boldsymbol{q}_{s_m}^n. \tag{8}$$

$\otimes$ is the quaternion multiplication operator. $\boldsymbol{p} \otimes \boldsymbol{q}$ is defined by $(p_0 + p_1 i + p_2 j + p_3 k)(q_0 + q_1 i + q_2 j + q_3 k)$ with the following properties:

$$i^2 = j^2 = k^2 = -1,$$
$$ij = -ji = k, \quad jk = -kj = i, \quad ki = -ik = j.$$

$\boldsymbol{q}_n^{s_1}$ is quaternion conjugate of $\boldsymbol{q}_{s_1}^n$ having the same first element as $\boldsymbol{q}_{s_1}^n$ but with the negative of elements 2 - 4 in $\boldsymbol{q}_{s_1}^n$.

The rotation axis is obtained from the orientation change quaternion $\boldsymbol{q}_{s_m}^{s_1}$ using the transformation between rotation vector and quaternion denoted as q2axis $(\cdot)$ in (9). The second line in (9) ensures that the rotation angle is between 0 to 180°.

$$\begin{cases} \boldsymbol{u} = \dfrac{\boldsymbol{q}(2:4)}{norm\,(\boldsymbol{q}\,(2:4))} & \text{if } 0 \le \boldsymbol{q}(1) < 1 \\ \boldsymbol{u} = \dfrac{-\boldsymbol{q}(2:4)}{norm\,(\boldsymbol{q}\,(2:4))} & \text{if } -1 < \boldsymbol{q}(1) < 0 \\ \boldsymbol{u} = [\,0 \quad 0 \quad 0\,]^T & \text{if } \boldsymbol{q}(1) = \pm 1 \end{cases} \tag{9}$$

The obtained unit vector of rotation axis $\boldsymbol{u}$ has exactly the same coordinate values in coordinate frame s_1 and s_m, i.e.,

$$\boldsymbol{u}^{\mathrm{s}1} = \boldsymbol{u}^{s_m} = \mathrm{q2axis}(\boldsymbol{q}_{s_m}^{s_1})$$

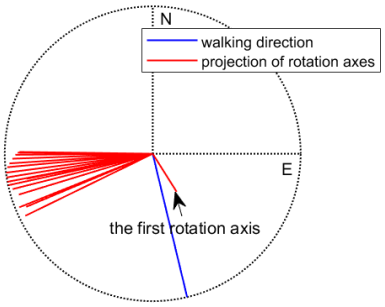

Fig. 8. Example of extracted rotation axes projection on horizontal plane.

Then the coordinate of rotation axis in navigation frame is given by (10).

$$\boldsymbol{u}^n = \boldsymbol{C}_{s_1}^n \boldsymbol{u}^{s_1} = \boldsymbol{C}_{s_m}^n \boldsymbol{u}^{s_m} \tag{10}$$

Fig.8 shows an example of the extracted rotation axes projection on horizontal plane during leg flexion. The circle with dotted line is the unit circle. The blue line indicates the walking direction.

Most of the extracted rotation axes are distributed around the orthogonal direction of walking direction. But first few axes are deviated from this distribution. In this example, the first rotation axis is significantly off the horizontal plane. This is because the orientation change between the start sample and the first few samples in leg flexion interval is relatively small and susceptible to interference. A threshold is designed to filter out the influence of these outliers. The final averaged rotation axis calculated in (11) comes from the rotation axes whose horizontal component magnitude is greater than 0.9.

$$\boldsymbol{u}_{\text{average}}^n = \frac{1}{M} \sum_{k=1,\mathrm{norm}(\boldsymbol{u}_k^n(1,2))>0.9}^{M} \boldsymbol{u}_k^n \tag{11}$$

At last, by rotating the horizontal projection of the averaged rotation axis 90° clockwise about the Up-axis using (12), the estimated direction cosine vector of heading is obtained.

$$\hat{\boldsymbol{\chi}} = \frac{\left[\, -\boldsymbol{u}_{\text{average}}^n(2) \quad \boldsymbol{u}_{\text{average}}^n(1) \,\right]^T}{\mathrm{norm}\left(\boldsymbol{u}_{\text{average}}^n\,(1,2)\right)} \tag{12}$$

The flowchart presented in Fig.9 summarizes the IRA algorithm for POCEKT mode.

D. Single-Point Method

For SWIMG mode, although the proposed IRA algorithm can also be applied to estimate the heading after the hand forward swing interval is detected, it is still expected to find a more computationally efficient method.

The smartphone swings beside the body just like a simple pendulum in SWING mode. Fig. 10 shows an example of the trajectory of y-axis's vertex on horizontal plane in SWING mode during one walking step. The circle with dotted line is the unit circle. The blue line represents the heading direction.

The x-y plane of smartphone is near the perpendicular plane. The horizontal projection of the y-axis is close to the walking direction, but not always on the same straight line. That's the

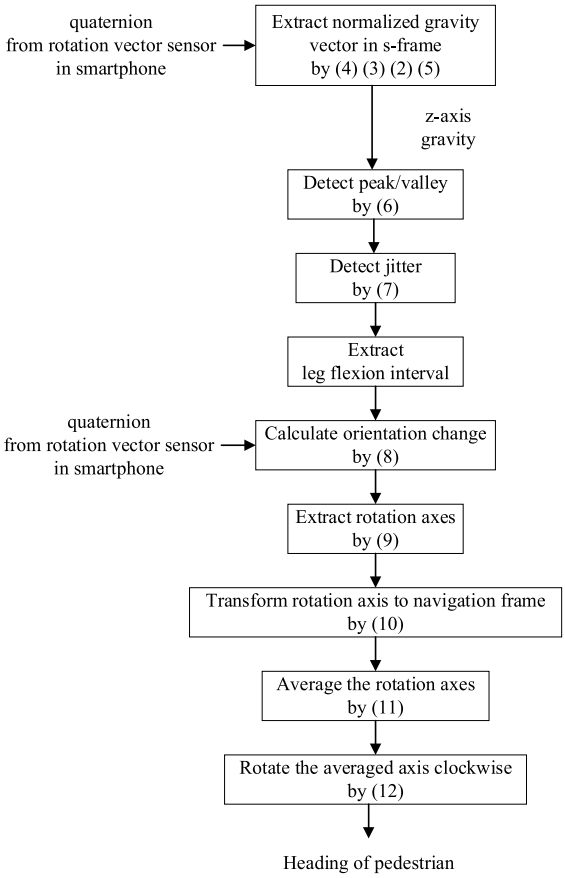

Fig. 9. Flowchart of IRA algorithm for POCEKT mode.

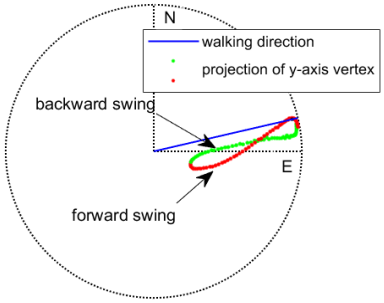

Fig. 10. Example of y-axis's vertex trajectory projection on horizontal plane.

reason why the yaw angle oscillates about the heading angle as mentioned in Section II. When y-axis is swung closest to the horizontal plane, the deviation between the yaw angle and the heading angle is minimal.

In our proposed single-point (SP) method, the heading is estimated from the direction of smartphone's y-axis when it is closest to the horizontal plane. The direction of y-axis is obtained from the rotation vector sensor according to the transformation between the quaternion and the direction cosine matrix in (4) (3) (2). The estimated direction cosine vector of pedestrian's heading is obtained by (13).

$$\begin{cases} \text{when } \mathrm{norm}(\boldsymbol{C}_s^n(:,2)) \text{ gets the maximum in one step} \\ \hat{\boldsymbol{\chi}} = \dfrac{\begin{bmatrix} \boldsymbol{C}_s^n(1,2) & \boldsymbol{C}_s^n(2,2) \end{bmatrix}^T}{\mathrm{norm}(\boldsymbol{C}_s^n(1:2,2))} \end{cases} \tag{13}$$

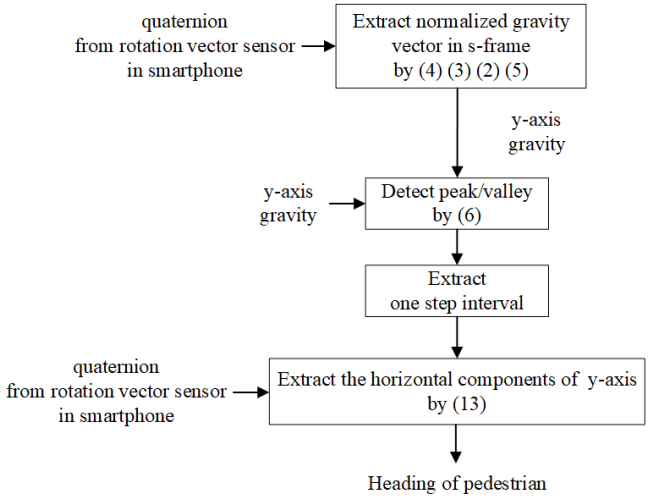

Fig. 11. Flowchart of SP algorithm for SWING mode.

The flowchart presented in Fig.11 summarizes the SP algorithm for SWING mode.

IV. Evaluation

A. Experiment Setup

To evaluate the performance of the proposed heading estimation algorithms, two trajectory patterns are tested for both POCKET and SWING modes. A straight-line pattern with more than 40 steps is used to evaluate the RMS error of heading estimation. A figure-of-eight pattern is used to evaluate the robustness of the algorithms.

For the straight-line pattern test, the test is implemented in a straight pedestrian street without cars. The straight line between the pavement tiles in the middle of the street is selected as our walking trajectory. During the experiments, the subjects keep treading on this straight line with natural gait. This ensures that the walking direction does not deviate from the reference direction. The true heading of this line is derived by a dual-frequency RTK GNSS receiver with fixed solutions. Although the heading derived from GNSS is respect to the true north, it should be noted that the attitude information provided by smartphone is respect to the magnetic north. Therefore, the reference heading is obtained by subtracting the local magnetic declination angle from the GNSS derived heading.

For the figure-of-eight pattern test, a waist-mounted 3DM-GX3-25 attitude and heading reference system (AHRS) is used to obtain the reference heading.

The smartphone data is collected by 2 subjects, one woman and one man, using Huawei mate 10 smartphone. The data rate is 50Hz.

In POCKET mode experiments, subjects put the smartphone in their front trouser pocket according to their own preference. Due to the shape of the smartphone and the pocket, the relative motion between smartphone and pocket is small during one experiment. Four algorithms are implemented to process the collected data. The proposed IRA algorithm only needs the rotation vector sensor measurement. The PCA2D and PCA2Df require accelerometer and rotation vector sensor. The PCA-GA processes accelerometer and magnetometer data.

TABLE I
POCKET MODE HEADING ESTIMATION COMPARISON

RMS error (°)	IRA	PCA2D	PCA2Df	PCA-GA
Subject 1	4.17	25.67	16.83	37.07
Subject 2	4.37	27.45	12.85	31.67

TABLE II
SWING MODE HEADING ESTIMATION COMPARISON

RMS error (°)	single-point	IRA	PCA2Df	PCA-GA
Subject 1	3.09	9.62	4.67	22.36
Subject 2	3.38	9.12	3.82	18.24

In SWING mode experiments, the smartphone is held with y-axis directing to the front of the hand. The SP method, IRA, PCA2Df and PCA-GA are implemented to process their required data.

B. Straight-Line Pattern Results

Heading estimation error χ_{error} is defined as the angle formed between the true heading direction cosine vector $\boldsymbol{\chi}$ and the estimated one $\hat{\boldsymbol{\chi}}$. χ_{error} is a signed error with its amplitude and sign determined by dot and cross product of direction vectors as in (14) and (15).

$$|\chi_{error}| = \arccos\left(\frac{\boldsymbol{\chi}\cdot\hat{\boldsymbol{\chi}}}{|\boldsymbol{\chi}|\,|\hat{\boldsymbol{\chi}}|}\right) \tag{14}$$

$$\text{sign}(\chi_{error}) = \text{sign}\left(\boldsymbol{\chi}\times\hat{\boldsymbol{\chi}}\right) \tag{15}$$

Heading estimation RMS error is defined as in (16)

$$RMS\ error = \sqrt{\frac{1}{M}\sum_{k=1}^{M}\left(\chi_{error,k}\right)^2} \tag{16}$$

where M is the step number under the carry mode to be evaluated.

The heel strikes, leg flexion intervals and forward swing intervals are correctly extracted for both data sets based on the proposed walking cycle state detection methods.

Table I and Table II show the heading estimation RMS error comparison of the tested algorithms under POCKET and SWING for each subject. For all the PCA-based methods, the 180° ambiguity in heading estimation is solved using direction consistent constraint so that the signed error is between $-90°$ to 90°.

In order to show the error distribution, boxplots of signed error are given in Fig. 12. In boxplot figure, the central mark indicates the median error and the bottom and top edges of the box indicate the 25th and 75th percentiles error, respectively. The '+' symbols extend to the most extreme boundary indicate outliers.

As seen from Table I, for POCKET mode, the IRA algorithm shows the minimum RMS error compared to the other three PCA-based methods. The PCA2Df implements low pass filter on the horizontal east and north acceleration before

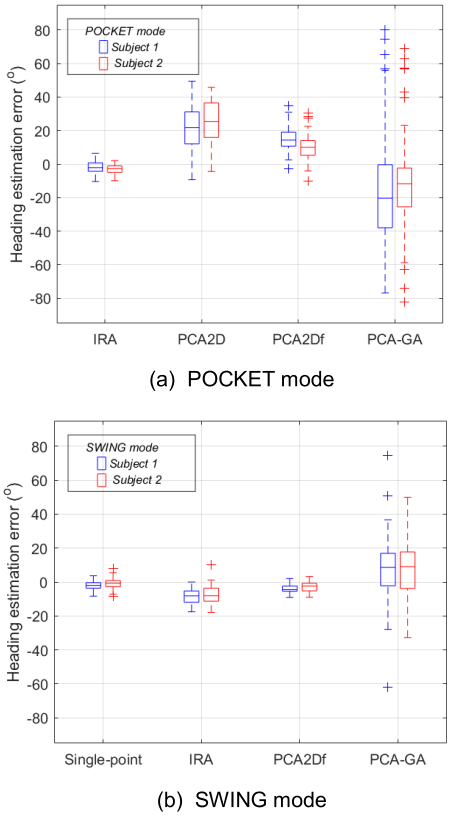

(a) POCKET mode

(b) SWING mode

Fig. 12. Signed estimation error distributions of compared algorithms.

principal component analysis. It seems that the RMS error of PCA2Df is less than PCA2D. However, from the signed error distribution boxplot shown in Fig.12 (a), neither of these two algorithms has a good convergence within one walking step. The PCA-GA shows the maximum RMS error because it is designed for the smartphone without gyroscope. It is impossible to reconstruct the accurate orientation of smartphone only using the accelerometer and magnetometer due to the influence of linear acceleration and magnetic field disturbance. Even though the PCA-GA gets a stable motion axis in smartphone frame which is approximately orthogonal to pedestrian's heading, the error is inevitable when transforming this axis into navigation frame.

Although all the three PCA-based methods do not provide satisfactory results for POCKET mode, the PCA2Df achieves good performance for SWING mode. As seen from Table II, the SP method proposed in this paper shows the minimum RMS error. The error performance of PCA2Df is a little worse than SP, but better than IRA and much better than PCA-GA. Fig. 12 (b) show that except PCA-GA, all the other three algorithms converge within single walking step.

The results of the original rotational approach (RA) are not shown in the previous result part. Because the rotation axes obtained based on the description of RA using our data are not as stable as the result shown in [21]. Actually, constructed by the orientation changes with a 0.5s interval, the distributions of continuous 50 rotation axe/angle samples are very scattered over positive and negative values. The weighted average process does not make the output estimation stable.

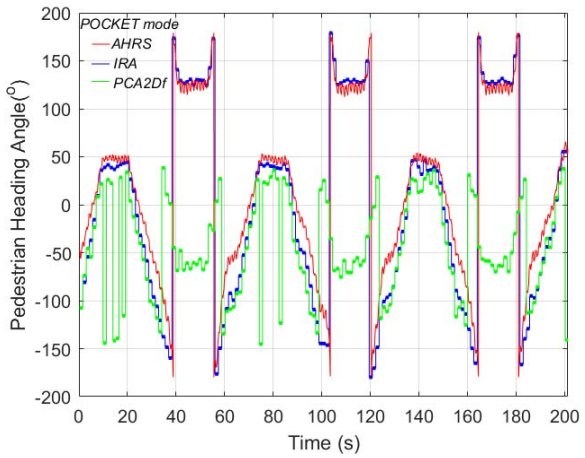

(a) POCKET mode

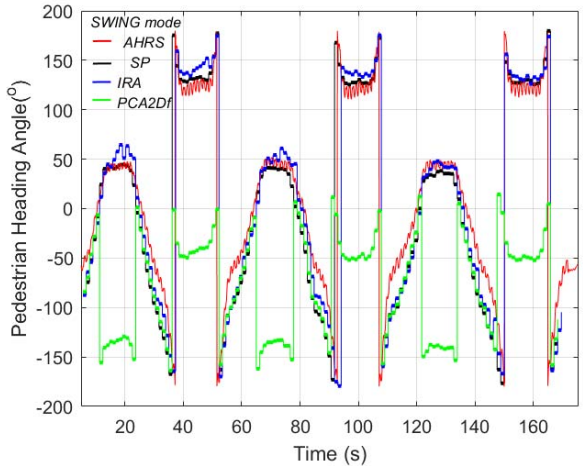

(b) SWING mode

Fig. 13. Heading estimation in the figure-of-eight pattern.

Our IRA improves the calculation of rotation axes by detecting leg flexion interval and hand forward swing interval and constructing the orientation change using the samples between the front boundaries and the subsequent ones in the interval.

C. Figure-of-Eight Pattern Results

Fig. 13 shows the heading estimation results in the figure-of-eight pattern. For the PCA2Df, the heading derived from the first eigenvector of the horizontal east and north accelerations is directly shown in Fig. 13 without 180° ambiguity correction.

The heading estimation performance of the straight-line parts in the figure-of-eight is consistent with the results in the VI-B. For the arc parts, the estimation performance decreases but still can track the reference heading to some extent. Moreover, our IRA and SP methods are able to determine the heading without 180° ambiguity. This is benefit from the detection of walking cycle states.

V. Conclusion

The main contributions of this paper are twofold. First, by using normalized gravity vector obtained from rotation vector sensor, human walking cycle states are detected under POCKET and SWING modes. This is novel in the sense that the walking step and heading estimation associated key intervals are extracted without complex threshold value selection. Second, compared to the existing heading estimation methods for multi-mode PDR system, the proposed IRA and SP algorithms are able to converge in one walking step. The estimation results are without 180° ambiguity.

Future work will be focused on extending the proposed heading estimation to the position solution for indoor pedestrian navigation by fusing other measurement such as WIFI fingerprint and building layout information.

References

[1] *Information Technology-Real Time Locating Systems-Test and Evaluation of Localization and Tracking Systems*, ISO/IEC document 18305, 2016.
[2] Q. Zeng, J. Wang, Q. Meng, X. Zhang, and S. Zeng, "Seamless pedestrian navigation methodology optimized for indoor/outdoor detection," *IEEE Sensors J.*, vol. 18, no. 1, pp. 363–374, Jan. 2018.
[3] H. Gao and P. D. Groves, "Environmental context detection for adaptive navigation using GNSS measurements from a smartphone," *Navigation*, vol. 65, no. 1, pp. 99–116, Mar. 2018.
[4] (2019). *Vicon Motion Tracking System*. [Online]. Available: http://www.vicon.com/
[5] H. Liu, H. Darabi, P. Banerjee, and J. Liu, "Survey of wireless indoor positioning techniques and systems," *IEEE Trans. Syst., Man, Cybern., C, Appl. Rev.*, vol. 37, no. 6, pp. 1067–1080, Nov. 2007.
[6] S. Godha and G. Lachapelle, "Foot mounted inertial system for pedestrian navigation," *Meas. Sci. Technol.*, vol. 19, no. 7, Jul. 2008, Art. no. 075202.
[7] S. Qiu, Z. Wang, H. Zhao, K. Qin, Z. Li, and H. Hu, "Inertial/magnetic sensors based pedestrian dead reckoning by means of multi-sensor fusion," *Inf. Fusion*, vol. 39, pp. 108–119, Jan. 2018.
[8] C. Huang, Z. Liao, and L. Zhao, "Synergism of INS and PDR in self-contained pedestrian tracking with a miniature sensor module," *IEEE Sensors J.*, vol. 10, no. 8, pp. 1349–1359, Aug. 2010.
[9] J. Lu, K. Chen, B. Li, and M. Dai, "Hybrid navigation method of INS/PDR based on action recognition," *IEEE Sensors J.*, vol. 18, no. 20, pp. 8541–8548, Oct. 2018.
[10] X. Meng, Z.-Q. Zhang, J.-K. Wu, W.-C. Wong, and H. Yu, "Self-contained pedestrian tracking during normal walking using an Inertial/Magnetic sensor module," *IEEE Trans. Biomed. Eng.*, vol. 61, no. 3, pp. 892–899, Mar. 2014.
[11] R. Harle, "A survey of indoor inertial positioning systems for pedestrians," *IEEE Commun. Surveys Tuts.*, vol. 15, no. 3, pp. 1281–1293, 3rd Quart., 2013.
[12] A. Martinelli, H. Gao, P. D. Groves, and S. Morosi, "Probabilistic context-aware step length estimation for pedestrian dead reckoning," *IEEE Sensors J.*, vol. 18, no. 4, pp. 1600–1611, Feb. 2018.
[13] W. Kang and Y. Han, "SmartPDR: smartphone-based pedestrian dead reckoning for indoor localization," *IEEE Sensors J.*, vol. 15, no. 5, pp. 2906–2916, May 2015.
[14] Z. Tian, Y. Zhang, M. Zhou, and Y. Liu, "Pedestrian dead reckoning for MARG navigation using a smartphone," *EURASIP J. Adv. Signal Process.*, vol. 2014, no. 1, p. 65, Dec. 2014.
[15] L.-F. Shi, Y. Wang, G.-X. Liu, S. Chen, Y.-L. Zhao, and Y.-F. Shi, "A fusion algorithm of indoor positioning based on PDR and RSS fingerprint," *IEEE Sensors J.*, vol. 18, no. 23, pp. 9691–9698, Dec. 2018.
[16] Y. Zhuang and N. El-Sheimy, "Tightly-coupled integration of WiFi and MEMS sensors on handheld devices for indoor pedestrian navigation," *IEEE Sensors J.*, vol. 16, no. 1, pp. 224–234, Jan. 2016.
[17] K.-C. Lan and W.-Y. Shih, "Using smart-phones and floor plans for indoor location tracking," *IEEE Trans. Human-Mach. Syst.*, vol. 44, no. 2, pp. 211–221, Apr. 2014.
[18] B. Zhou, Q. Li, Q. Mao, W. Tu, and X. Zhang, "Activity sequence-based indoor pedestrian localization using smartphones," *IEEE Trans. Human-Mach. Syst.*, vol. 45, no. 5, pp. 562–574, Oct. 2015.
[19] H. Zhang, W. Yuan, Q. Shen, T. Li, and H. Chang, "A handheld inertial pedestrian navigation system with accurate step modes and device poses recognition," *IEEE Sensors J.*, vol. 15, no. 3, pp. 1421–1429, Mar. 2015.

[20] Q. Tian, Z. Salcic, K. I.-K. Wang, and Y. Pan, "A multi-mode dead reckoning system for pedestrian tracking using smartphones," *IEEE Sensors J.*, vol. 16, no. 7, pp. 2079–2093, Apr. 2016.
[21] U. Steinhoff and B. Schiele, "Dead reckoning from the pocket–An experimental study," in *Proc. IEEE Int. Conf. Pervas. Comput. Commun. (PerCom)*, Mar. 2010, pp. 162–170.
[22] K. Kunze, P. Lukowicz, K. Partridge, and B. Begole, "Which way am i facing: Inferring horizontal device orientation from an accelerometer signal," in *Proc. Int. Symp. Wearable Comput.*, Sep. 2009, pp. 149–150.
[23] B. Wang, X. Liu, B. Yu, R. Jia, and X. Gan, "Pedestrian dead reckoning based on motion mode recognition using a smartphone," *Sensors*, vol. 18, no. 6, p. 1811, 2018.
[24] (2019). *Android Developers-Motion Sensors*. [Online]. Available: https://developer.android.com/guide/topics/sensors/sensors_motion
[25] P. G. Savage, "Strapdown inertial navigation integration algorithm design part 1: Attitude algorithms," *J. Guid., Control, Dyn.*, vol. 21, no. 1, pp. 19–28, Jan. 1998.
[26] H. Cheng and K. C. Gupta, "An historical note on finite rotations," *J. Appl. Mech.*, vol. 56, no. 1, pp. 139–145, Mar. 1989.
[27] S. O. H. Madgwick, A. J. L. Harrison, and R. Vaidyanathan, "Estimation of IMU and MARG orientation using a gradient descent algorithm," in *Proc. IEEE Int. Conf. Rehabil. Robot.*, Jun. 2011, pp. 1–7.
[28] R. Mahony, T. Hamel, and J.-M. Pflimlin, "Nonlinear complementary filters on the special orthogonal group," *IEEE Trans. Autom. Control*, vol. 53, no. 5, pp. 1203–1218, Jun. 2008.
[29] J. Wu, Z. Zhou, J. Chen, H. Fourati, and R. Li, "Fast complementary filter for attitude estimation using low-cost MARG sensors," *IEEE Sensors J.*, vol. 16, no. 18, pp. 6997–7007, Sep. 2016.
[30] D. Mizell, "Using gravity to estimate accelerometer orientation," in *Proc. 7th IEEE Int. Symp. Wearable Comput.*, Oct. 2003, pp. 252–253.

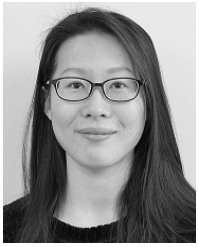

Lingxiao Zheng received the B.S. degree in communication engineering from Yanshan University, China, in 2011, and the M.S. degree in control science and engineering from Shanghai Jiao Tong University, China, in 2014, where she is currently pursuing the Ph.D. degree. Her research interests include pedestrian dead reckoning, visible light communication-based positioning, vision-based positioning, multisource indoor outdoor seamless positioning, and sensor fusion algorithm.

Xingqun Zhan (Senior Member, IEEE) received the B.S. and M.S. degrees from Harbin Engineering University, in 1992 and 1994, respectively, and the Ph.D. degree from the Harbin Institute of Technology in 1999. He is currently a Professor and the Associate Dean of the School of Aeronautics and Astronautics, Shanghai Jiao Tong University, where he conducts the Guidance, Navigation and Control Laboratory. His research interests include GNSS compatibility/interoperability and vulnerability evaluation, GNSS/INS ultra-tightly coupled integration, seamless positioning, and multisensor integration. He serves as an Expert Panel Member of the BeiDou Program, and is selected as a member of the Chinese National Ten-Thousand Talent Program. He is co-chairing the Application Subgroup of International Committee of GNSS (ICG) under UNOOSA. He is an Associate Fellow of the AIAA, and an Associate Editor of *Aerospace Science and Technology*.

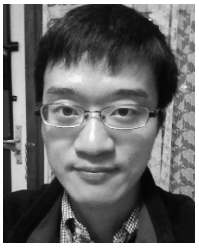

Xin Zhang received the B.S. (Hons.) degree in telecommunications engineering from Dong Hua University, China, in 2003, and the M.S. and Ph.D. degrees in guidance, navigation, and control from Shanghai Jiao Tong University, in 2008 and 2013, respectively. He holds a second level specializing master's (Hons.) degree in navigation and related applications from Politecnico di Torino, Italy. He was an Intern with the Navigation Division, Thales Alenia Space Italia, Milan. He is an Assistant Professor with the School of Aeronautics and Astronautics, Shanghai Jiao Tong University. His research interests include vector tracking GPS receivers, INS/GPS deep integration, and all-source navigation and positioning.

Shizhuang Wang (Member, IEEE) received the B.S. degree in aerospace engineering from Shanghai Jiao Tong University (SJTU), China, in 2018, where he is currently pursuing the master's degree with the School of Aeronautics and Astronautics. His research interests focus on multisensor integration, fault detection and exclusion, and integrity monitoring. He received the Shanghai Excellent Graduate Student Award and the SJTU Excellent Bachelor Thesis Award (Top 1%). He acts as a Reviewer for *Aerospace Science and Technology* and *Aerospace Systems*.

Wenhan Yuan received the B.A.Sc. degree in aeronautics and astronautics engineering from Shanghai Jiao Tong University, Shanghai, China, in 2014, where he is currently pursuing the Ph.D. degree. His research interests include vision-based indoor localization and multisensor indoor localization systems, such as WIFI and IMUs.